Prompt Optical Emission from Gamma-ray Bursts

By Robert Kehoe[1], Carl Akerlof[1], Richard Balsano[2], Scott Barthelmy[3,4], Jeff Bloch[2], Paul Butterworth[3,5], Don Casperson[2], Tom Cline[3], Sandra Fletcher[2], Fillippo Frontera[6], Galen Gisler[2], John Heise[7], Jack Hills[2], Kevin Hurley[8], Brian Lee[1], Stuart Marshall[9], Tim McKay[1], Andrew Pawl[1], Luigi Piro[10], Bill Priedhorsky[2], John Szymanski[2] and Jim Wren[2]

[1]University of Michigan, Ann Arbor, MI 48109, USA

[2]Los Alamos National Laboratory, Los Alamos, NM 87545, USA

[3]NASA/Goddard Space Flight Center, Greenbelt, MD 20771, USA

[4]Universities Space Research Association, Seabrook, MD 20706, USA

[5]Raytheon Systems, Lanham, MD 20706, USA

[6]Università degli Studi di Ferrara, Ferrara, Italy

[7]Space Research Organization, Utrecht, The Netherlands

[8]Space Sciences Laboratory, University of California, Berkeley, CA 94720-7450, USA

[9]Lawrence Livermore National Laboratory, Livermore, CA 94550, USA

[10]Instituto Astrofisica Spaziale, Rome, Italy

The Robotic Optical Transient Search Experiment (ROTSE) seeks to measure contemporaneous and early afterglow optical emission from gamma-ray bursts (GRBs). The ROTSE-I telescope array has been fully automated and responding to burst alerts from the GRB Coordinates Network since March 1998, taking prompt optical data for 30 bursts in its first year. We will briefly review observations of GRB990123 which revealed the first detection of an optical burst occurring during the gamma-ray emission, reaching 9th magnitude at its peak. In addition, we present here preliminary optical results for seven other gamma-ray bursts. No other optical counterparts were seen in this analysis, and the best limiting sensitivities are $m_V > 13.0$ at 14.7 seconds after the gamma-ray rise, and $m_V > 16.4$ at 62 minutes. These are the most stringent limits obtained for GRB optical counterpart brightness in the first hour after the burst. This analysis suggests that there is not a strong correlation between optical flux and gamma-ray emission.

1. Introduction

1.1. *Gamma-ray Observations*

Fast, intense bursts of cosmic gamma-rays and energetic X-rays were first observed about 30 years ago (Klebesadel et al. (1973)). Since that time, satellite missions have determined several characteristics of these events. They are generally very brief but are otherwise extremely diverse in their gamma-ray temporal variations. Durations range from 0.005 to 100's of seconds, and intensity fluctuations are as short as 0.3 ms (Hurley et al. (1984)). They are often instantaneously the brightest gamma-ray source in the sky. Studies of the over 2000 currently recorded bursts indicate a thoroughly isotropic distribution with no detectable concentration towards the galactic plane and no angular correlations with other astrophysical structures (Meegan et al. (1998)).

1.2. *Counterparts at Other Wavelengths*

Given the lack of a spatial or temporal pattern, it has been extremely difficult to comprehend the physical mechanisms from the gamma-ray observations alone. Since the mid-70s, there have been many attempts to detect counterparts at other wavelengths, but they were unsuccessful until 1997. The difficulty arose from the brevity of bursts, the lack of arc-minute localizations and theoretical prejudices concerning the burst progenitor. Currently, the two main GRB efforts utilize the BATSE detectors (Fishman et al. (1989)) on-board the Compton Gamma-Ray Observatory, and the GRBM (Feroci et al. (1997)) and WFC (Jager et al. (1997)) on the BeppoSAX satellite, and they have addressed the observational limitations very differently. BATSE's advantage is its near complete coverage of the sky, which allows observation of about 300 bursts per year, and its unique ability to provide rough coordinates very rapidly ($\sim$ 5 seconds). These localizations are distributed in the form of triggers over the GRB Coordinates Network (GCN) (Barthelmy et al. (1998), Barthelmy et al. (1995)). Beppo-SAX, on the other hand, is able to deliver positions accurate to a few arcminutes in a few hours for about a dozen bursts per year.

The BeppoSAX positions are accurate enough for follow-up with conventional, small field-of-view telescopes which have detected optical counterparts for twelve GRBs. As a result, we now know that at least some GRBs are at cosmological distance (eg. Metzger et al. (1997), Kulkarni et al. (1998)) and, if their emission is isotropic, release a significant fraction of $M_{\odot}c^2$. These GRBs, at least, are associated with galaxies (Hogg and Fruchter (1999)). Studying this afterglow period of a few hours to days after the burst has generally revealed a slow, roughly power-law decay of optical emission with time.

These observations, however, are mute concerning the details of the burst itself, and there are several limitations in the current sample. In particular, the number of such events is small. There is also a bias which arises from the requirement of an observable X-ray counterpart. In addition, because the BeppoSAX GRBM uses a 1 second integration period, no counterparts at any wavelength have been identified for the class of short ($\sim$ 0.1 second) bursts. Short bursts are more likely to have high energy emission, and they occupy a region of the hardness-ratio vs. duration space well-separated from long bursts (Kouveliotou et al. (1993), Kouveliotou et al. (1996)). This may imply a different type of progenitor for short bursts. Lastly, these observations occur hours after any gamma-ray emission, so that despite a growing understanding of afterglows, the burst origin remains a mystery.

1.3. *Prompt, Unbiased Optical Detections*

Studying early optical emission in an unbiased way has several advantages. First, observations at early times may elucidate details of shock development, the burst environment and beaming. Second, by looking for optical emission unbiased by selections based on burst duration or fluence, we can probe more thoroughly their range of behavior.

While we do not know the actual mechanism by which a GRB occurs, there is a general picture of the development of the cataclysm aftermath. A highly relativistic expanding fireball is created in which shells develop within the outflow with a spread in velocities. Gamma-rays emerge from interactions among these shells (Rees and Meszaros (1994), Paczynski and Xu (1994)). The chaotic time histories of the gamma-rays favor variability from a central engine such as in the internal shock models (Fenimore et al. (1996)). As the relativistic shell propagates into the interstellar medium, its deceleration produces a forward shock wave (Rees and Meszaros (1992), Meszaros and Rees (1993)) and possibly a reverse shock. The afterglow is believed to arise from the forward shock, while

significant early optical emission may arise from the reverse shock. In this scenario, comparisons of simultaneous optical and gamma-ray emission comment on the presence and progress of the external shocks. For instance, the relative timing of optical and gamma-ray emission indicates the Lorentz factors involved (Sari and Piran (1999)) as well as the process by which the shells responsible for the external shocks arise.

In addition, we can learn about the environment of the source at the time of the burst. The detectability of optical emission alone demonstrates that the local environment of the burst is not opaque to optical photons.

Since the relativistic shell is initially moving at very high bulk Lorentz factors, $\Gamma > 100$, there will be a beaming angle which is expected to vary roughly as $1/\Gamma$. If the optical photons arise from a more slowly moving region than the gamma-rays, they will be more isotropically emitted. This can occur, for instance, in the case of later optical emission from the decelerating relativistic shell. As a result, the correlation between this optical emission and the gamma-rays will be weak and we could observe a bright optical counterpart to a dim or absent gamma-ray burst (Rhoads (1999)). In addition, the energy release of a GRB might not be isotropic, being restricted to a jet of angular width, θ. This restriction will dominate the optical emission once $\Gamma \sim 1/\theta$. After some time, however, there will be lateral spreading of the jet which will further increase the isotropic distribution of the later optical light (Rhoads (1999)).

Any detection of optical emission from short bursts could reveal their relation to the longer bursts. The short bursts may have a different redshift distribution than that observed for long bursts. The two populations might arise from very different sources, such as neutron star mergers and hypernovae. If so, they should have distinct distributions within galaxies, and their local environments might be quite different. The fireball mechanism may be entirely different for short bursts. If so, prompt optical observations should help illuminate their properties.

2. The ROTSE Project

2.1. *Challenges*

To probe the nature of GRBs, the ROTSE project seeks to detect their prompt optical emission. In particular, we wish to detect optical photons coincident with a burst and observe optical afterglows to a few hours afterwards. Ultimately, we wish to do this for a sample of GRBs as free of detection biases as possible. We have a secondary mission to obtain and provide a stream of arcsecond-level positions for many GRBs for more sensitive follow-up.

To do this, several technical challenges must be met. First, the gamma-ray emission lasts a few seconds or less so we need to respond to triggers for gamma-ray bursts in real-time. Second, they vary rapidly during their gamma-ray emission and might be expected to do the same in the optical. Therefore, we must frequently image GRB positions to measure short time-scale variation. All of this requires a fully automated system. Third, the field-of-view of the instrument must match the positional accuracy of the trigger which, for BATSE coordinates, is 5 to 20 degrees. While this is far larger than the field-of-view of conventional optical telescopes, it is achievable in a moderately sensitive ($m_V \sim 15$) configuration. Finally, for analysis purposes, we must be able to distinguish rare signals from a variety of backgrounds.

We have developed a compact, flexible design consisting of fully automated mini-observatories. In the rest of Section 2, we discuss the technical details of our experiment, Section 3 outlines the operation of ROTSE-I, Section 4 reviews the observations

of GRB990123, Section 5 presents results on several other GRBs, and Section 6 presents an interpretation of those results.

2.2. *Mini Observatories*

The ROTSE telescopes are sited in northern New Mexico inside enclosures providing for the control and protection of the hardware. These enclosures possess an automatable enclosure cover ('clamshell'). In general, they are instrumented with weather sensors to detect rain, clouds, temperature, humidity, and excessive wind. In addition, lightning is a serious hazard at the site, so surge suppressors must protect all electrical lines to the outside world. Uninterruptible power supplies (UPSs) perform some power-line filtering and provide about 10 minutes of power to gracefully shut down the system in case of power failure. Each enclosure's internal network and external connection runs on 100 Mbps ethernet. At the moment, the site itself is limited to a 10 Mbps connection.

Within the enclosures, there are computers and a custom control box for operation and monitoring of the various devices. The control box provides power to the telescope mount, clamshell, and the weather monitoring devices, as well as communication to the weather devices and clamshell. One of the keys to performing our experiment is the utilization of fast, inexpensive PCs. The division of labor among the computers in the enclosures varies, but in general there is a main computer on which our data acquisition system runs. This includes monitoring the weather devices, incoming triggers and system errors, control of the clamshell, and observation scheduling. Operation of the mount and data processing may also occur from this computer. Each camera is interfaced to an auxiliary PC via an ISA card interface.

Our data storage needs are handled by the the Los Alamos Computing Division Mass Store System. This storage system has a several Petabyte capacity, and provides crucial random access to our large data set via a quick and convenient interface.

2.3. *Software Components*

To achieve prompt response times and maximum livetime, each instrument must be automated, and it must operate in real-time. We chose Linux based on its stability, capability and cost, as well as the avilability of drivers and other software parts necessary for the experiment. Although Linux was not inherently designed for real-time application, we can tolerate 0.1 second latencies in responsiveness which is well within the operating system's capabilities.

We have produced a small suite of programs as diagrammed in Figure 1. The overall structure of the system consists of a central switchboard process which channels *commands* from user input processes to hardware control programs via shared data structures. This switchboard also relays *status* information from the hardware control and monitoring programs (ie. camera, mount, clamshell, GCN monitor, weather monitor, and watchdog) back to the users. The two user processes are an astronomical scheduler for automation and a modified UNIX shell for manual control. Aside from small portions directly interfacing to specific hardware, we have designed a simple, general structure for easy porting to newer systems as we develop them. A large effort has been made to produce a responsive system, so we have taken maximum advantage of Linux's interrupting and multitasking capabilities.

In order to be sure of the absolute timing of events, the main computer is synchronized to public servers using the Network Time Protocol (NTP), and the camera computers are synchronized to the main computer also via NTP. This configuration maintains the main computer within 10 ms of UTC and the camera computers within about 1 ms of the main computer and each other.

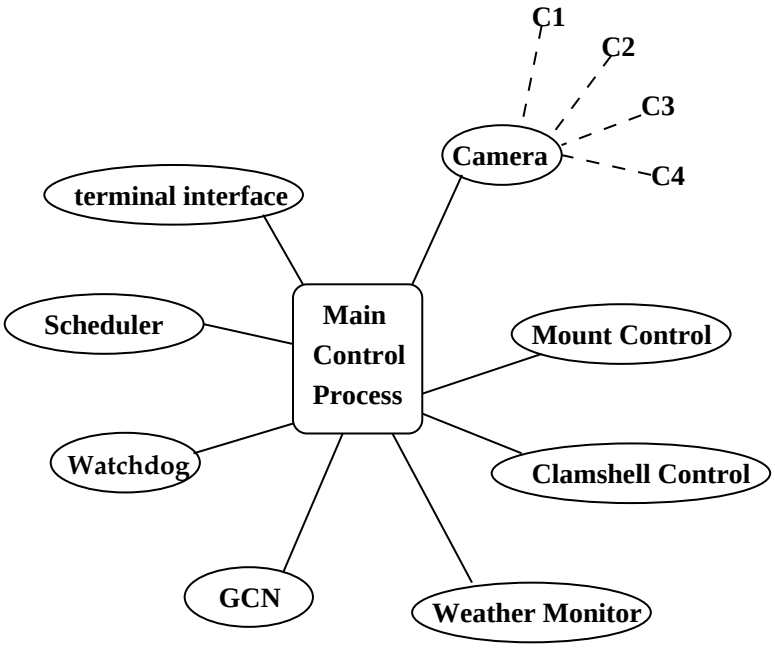

FIGURE 1. Scheme of ROTSE data-acquisition system. A central switchboard process running on the control computer channels commands from a user interface and scheduler to hardware control processes via shared data channels (solid lines). The instantaneous status of these processes and other monitors is continuously returned. Four additional PCs are used to control the four CCD cameras, with communication with the main computer proceeding over network connections (dashed lines).

2.4. *Telescopes*

We have developed a two-tiered program to cover the initial outburst and afterglow periods. ROTSE-I is fast, wide field-of-view, and moderately sensitive. It consists of a 2×2 array of small telescopes co-mounted on a rapid-slewing platform (see Figure 2). Each telescope is instrumented with a thermoelectrically cooled CCD camera employing a 14-bit Thompson TH7899M chip with 2048×2048 14 micron pixels. Read noise is $\sim 25e^-$, and readout is limited by the ISA interface to take about 7 seconds. The optics of each telescope consist of a Canon FD 200 mm $f/1.8$ telephoto lens. We have equipped each with a focus-ring clamp positioned by a micrometer for accurate manual adjustment. Our sensitivity to faint point sources is maximized by the match of the optical point spread function to the pixel size. The plate scale for ROTSE-I images is 14.4"/pixel. To further improve sensitivity, the cameras are operated without filters, and the peak response is in the R, V and I bands. Each telescope is sensitive to 14th magnitude in a 5 second exposure, and the array covers a $16.4^\circ \times 16.4^\circ$ field-of-view. The mount is capable of slewing to any point in the sky in less than 3 seconds. As shown in Figure 3, ROTSE-I is capable of seeing optical counterparts as dim as 14th magnitude by 10 seconds after a burst, and longer exposures achieve 16th magnitude sensitivity.

The second stage of the experiment brings significant improvements in sensitivity to faint objects. Each of the two existing ROTSE-II telescopes consists of a wide-field modified Cassegrain optical tube instrumented with the same cameras as ROTSE-I and a

FIGURE 2. The ROTSE-I telephoto array. Four Canon lenses are each mounted on CCD cameras on a compact, fast mount. The telescope sits on the roof of the ROTSE-I enclosure.

mount with an average slew time of 15 seconds. We have started building an additional set of eight similar telescopes, called ROTSE-III, with improved optics, back-illuminated CCD chips, and substantially faster slew times. All of these consist of $f/1.9$ optical assemblies with 45 cm apertures and 1.9° field-of-view. The plate scale is 3.4"/pixel. With these telescopes, we will study optical bursts for those few, prompt, accurate localizations from HETE2 (Ricker et al. (1990)), and we will observe optical afterglows by scanning the neighborhood of BATSE burst locations. We will also search for non-triggered fast-fading optical transients which might have a similar physical origin. The estimated sensitivity of these instruments is shown in Figure 3.

3. ROTSE-I Operations

3.1. *Observation Scheduling*

The astronomical scheduler is responsible for starting and stopping a night's run, designing observing sequences during the night, and scheduling darks for image noise correction. There are currently two main observing modes. Most of the time is spent in a lower priority sky patrol. Given the ROTSE-I field-of-view, 206 frames cover the celestial sphere with reasonable overlaps. We observe all fields with elevation $> 20°$ in two successive images taken twice nightly. These images were 25 second exposures until December 1998, and generally 80 seconds since then. These data are valuable for untriggered transient

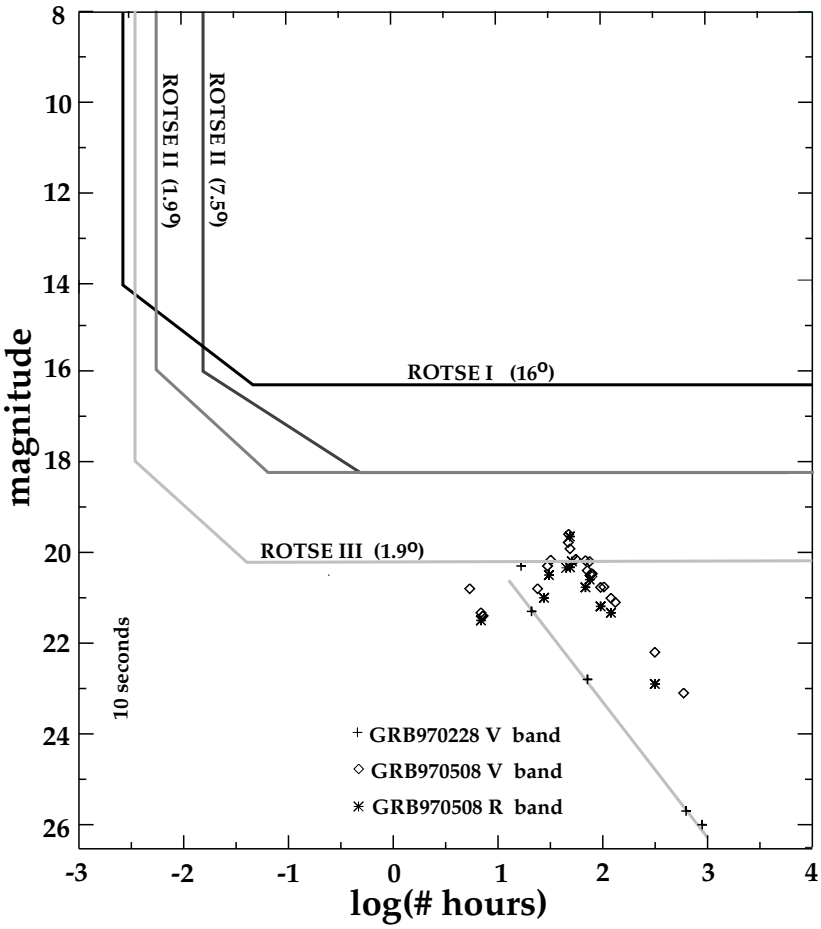

FIGURE 3. Sensitivity of ROTSE instruments vs. delay time. ROTSE-I's limiting sensitivity is 14th to 16th magnitude depending on exposure length, ROTSE-II goes approximately two magnitudes deeper, and ROTSE-III goes four magnitudes deeper. The field-of-view of each configuration is given in parentheses (7.5° for ROTSE-II is with tiling). Afterglow points for the first two optical counterparts are shown for comparison (see Galama et al. (1998), Fruchter et al. (1998), Pedersen et al. (1998a)).

studies and calibrations. They also provide precursor images for GRB fields and permit studies of the optical transient background.

About once per week, an observable trigger is received via GCN, and in these instances we interrupt any ongoing sky patrol observations for the higher priority alert. A response is scheduled which depends on the trigger coordinates and type. Different trigger types arrive with different transient position errors as well as different delays from the initial event detection. About half of all triggers received correspond to classic GRBs. In general, a series of exposures with increasing durations is taken as the response progresses. Until December 1998 we employed exposure lengths of 5, 25 and 125 seconds, then changed briefly to 5, 75, and 200 seconds, and since January we have used 5, 20, and 80 seconds. If we are observing the burst within seconds of its rise, we take short exposures

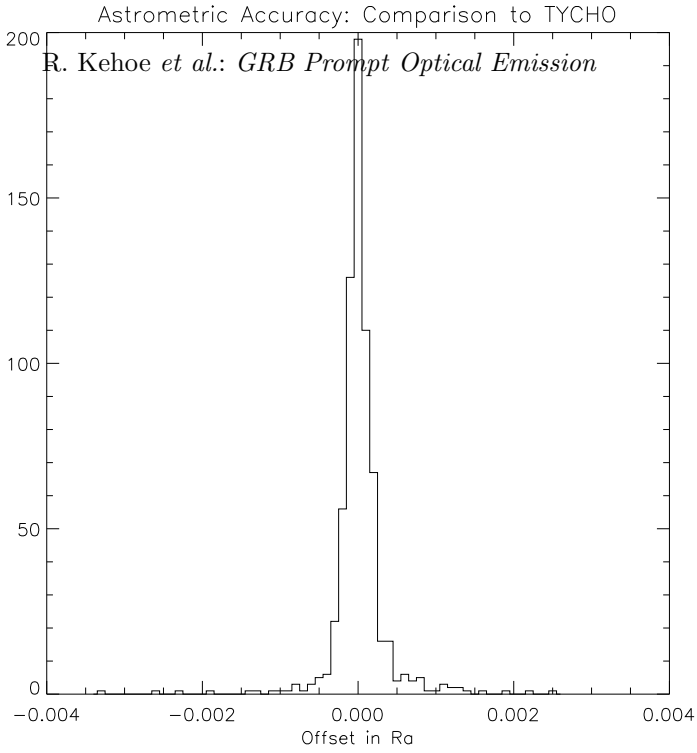

FIGURE 4. RA residuals in degrees for calibrated objects identified in ROTSE-I images compared to Hipparcos coordinates. Centroids are accurate to 1.4 arcecond (ie. 0.1 pixel).

initially. Longer delays begin with longer exposures. If the trigger is of a type with a large position error, then we also 'tile' around the given position ($32^\circ \times 32^\circ$) at specific points in the sequence. In this case, several direct-pointing images are taken and then a pair of images is taken in each of the four corners around the trigger coordinates. We then return to the direct pointing with longer exposures and begin the sequence again.

3.2. *Online Data Processing*

Every observing night, multiple raw darks are taken for each exposure length and averaged to produce a reference dark. Flats are produced by dark-subtracting and median-averaging ~ 60 sky patrol frames. For the most part, the flat variation is dominated by vignetting which amounts to a 60% loss at the frame corners. The process of making flats and darks also generates diagnostics which are regularly examined for signs of hardware problems. These correction frames are applied to the rest of the data to compensate for CCD noise and photometric response variations. After the correction procedure, images are reduced to lists of objects using SExtractor (Bertin and Arnouts (1996)) which provides rough photometry and cluster shape information. Due to processing and data transfer limitations, only the triggered data and some of the sky patrol data can currently be processed online. Once a night's observing is done, the data is moved automatically to mass storage.

3.3. *Astrometry and Photometry*

We currently perform our final astrometric and photometric calibrations offline by comparing our raw object lists to Hipparcos data (Høg et al. (1998)). Photometry is established by comparing raw ROTSE magnitudes to V-band measures and color correcting based on B-V. Astrometry is determined by triangle-matching approximately 1000 cat-

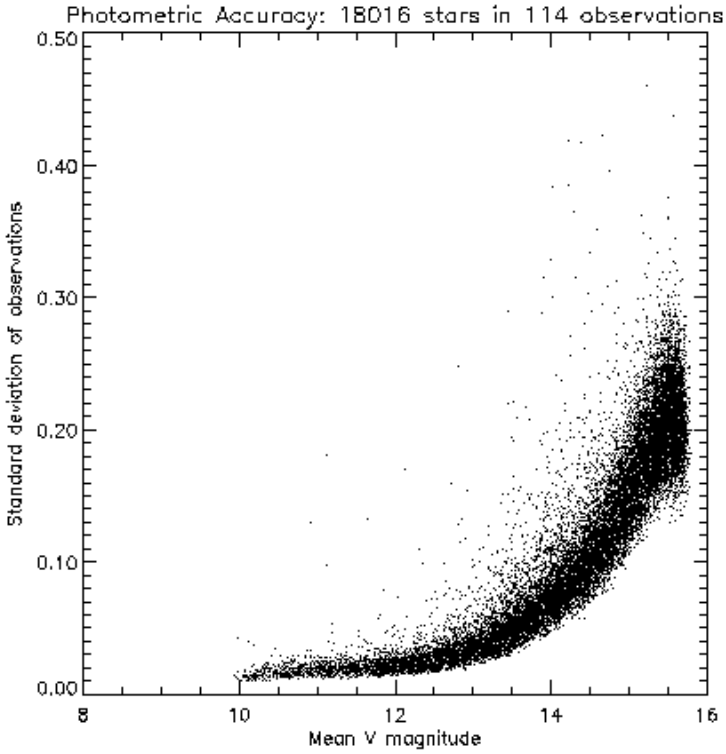

FIGURE 5. Magnitude residuals for calibrated objects identified in ROTSE-I images compared to Hipparcos photometry. Our final final photometric errors are ~ 0.02 magnitude for bright stars.

alog stars to each image, and determining warp corrections via a third order polynomial fit. As shown in Figure 4, our astrometric errors are 1.4 arcsec, and Figure 5 indicates our photometric errors to be as good as 0.02 magnitude for bright stars.

3.4. *Run Summary*

ROTSE-I operations achieved robust automation in March 1998, and during the first 12 months observed approximately 75% of all nights. The downtime resulted from very bad weather and from occasional hardware and software failures. In a typical night, the entire visible sky is imaged to 15th magnitude four times. In the first year, every field north of declination $-30°$ was observed between 200 and 900 times. The data stream is approximately 8 Gb/day, and the total amount of data generated is currently > 2 Tb. In that time, ROTSE-I responded to 49 physically interesting triggers. Of these, 30 were from classic gamma-ray bursts, 13 were from soft gamma-ray repeater events (10 of SGR1900+14), and 6 were X-ray transients. Response times for the subsample of prompt GRB and SGR triggers are shown in Figure 6.

4. Contemporaneous Optical Emission from GRB990123

At approximately 9:47 UTC on Jan 23, 1999, BATSE and Beppo-SAX triggered on an intense GRB. After 4 seconds, ROTSE received the estimated GCN coordinates (see

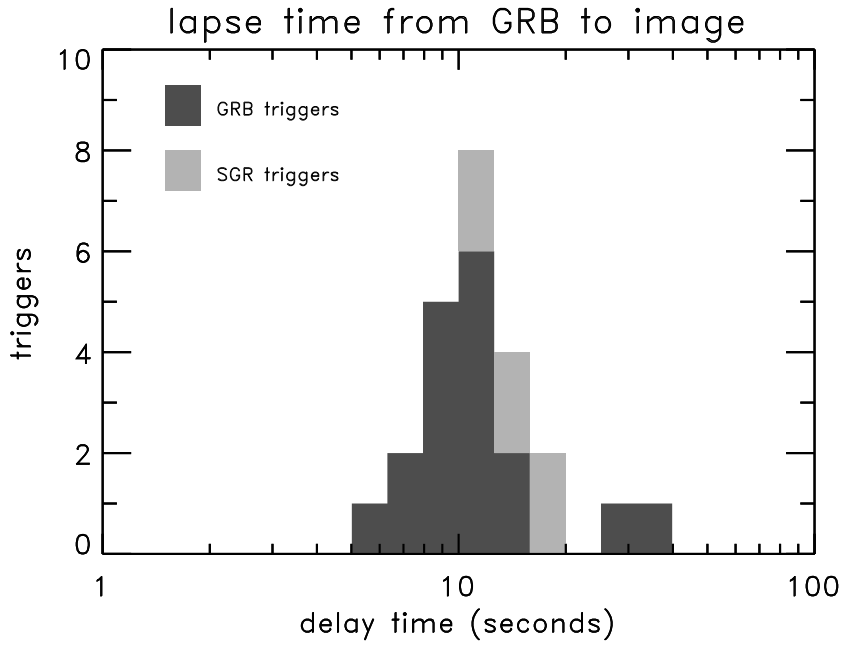

FIGURE 6. Delays for prompt GRB triggers. Times refer to period between the gamma-ray rise and the opening of the shutter for the first ROTSE-I exposure. The typical delay time is 10 seconds.

Figure 7), and scheduled an observational sequence which began the first exposure after another 6 seconds. One hundred minutes and 200 images later, the ROTSE trigger response was complete. In about 4 hours, the Beppo-SAX position, accurate to 0.1°, became available (Piro et al. (1999)), leading to the detection of the optical afterglow (Odewahn et al. (1999)). It also permitted quick identification of a burst of optical photons in the ROTSE images spatially coincident with the optical afterglow (see Figure 8). As shown in Figure 9, this 'optical burst' was surprisingly bright, reaching 9th magnitude at its peak 50 seconds after the gamma-ray rise (Akerlof et al. (1999)).

The observations of GRB990123 demonstrate several things about gamma-ray bursts. First, some subset of GRBs do exhibit optical bursts with fluctuations as violent as the gamma-ray variations (see inset in Figure 9). This observation and the optical brightness of the event imply that optically absorbing material local to the event was minimal.

The fact that the optical and gamma-ray emission were both intense and similarly short-lived suggests that the two are connected. On the other hand, while the gaps between the optical observations do not permit an exact location of the optical peak, it clearly did not occur when the gamma-rays were at maximum, thereby suggesting the gamma-rays and optical emission came from different processes in the burst. In particular, the observations are consistent with coming from a reverse shock (Sari and Piran (1999)).

When considering the measured redshift, $z = 1.6$, of this GRB (Kelson et al. (1999), Hjorth et al. (1999)), it becomes evident that this is a truly collossal event. In optical light, it is the most luminous object ever recorded, having a peak absolute magnitude of -36.4. Assuming isotropy, over $M_{\odot}c^2$ was released in gamma-rays. Such an energy output

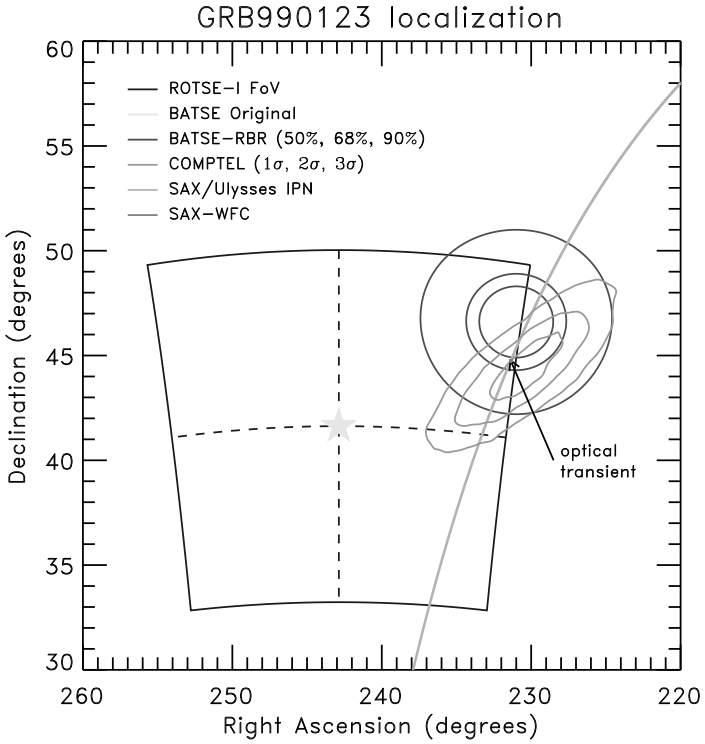

FIGURE 7. Various localizations of GRB990123 superimposed on ROTSE-I field-of-view. The optical counterpart was within 0.1° of the frame edge.

is large enough to cause great difficulty for most GRB models, which typically provide only about 1% of the inferred energy (see Janka and Ruffert (1996), Ruffert et al. (1997) and Meszaros and Rees (1997) and references within). This has led to speculation that the emission is not isotropic, suggesting a beaming scenario (Kulkarni et al. (1999)).

5. What About Other Bursts?

5.1. *Strategies*

The gamma-ray fluence of GRB990123 is about 100 times that of a median BATSE burst. If there is a strong linear correlation between gamma-ray fluence and optical flux, ROTSE-I should be sensitive enough to find optical counterparts to roughly half of the GRBs observed. Our ongoing analysis of seven earlier bursts (see Table 1) might then be expected to reveal more optical counterparts.

We have simplified the analysis by choosing those with the smallest position errors – six of the seven possess square-degree level localizations or better, while one (GRB980527) has a BATSE statistical error of about 1.1°. This results in an enormous reduction in background ($> 200\times$). Aside from the one BeppoSAX position for GRB980329a, the more accurate positions arise from the use of the gamma-ray detectors on-board Ulysses (Hurley et al. (1999)). By comparing timing information between two widely spaced detectors, thin annuli are generated which are several degrees long but only about

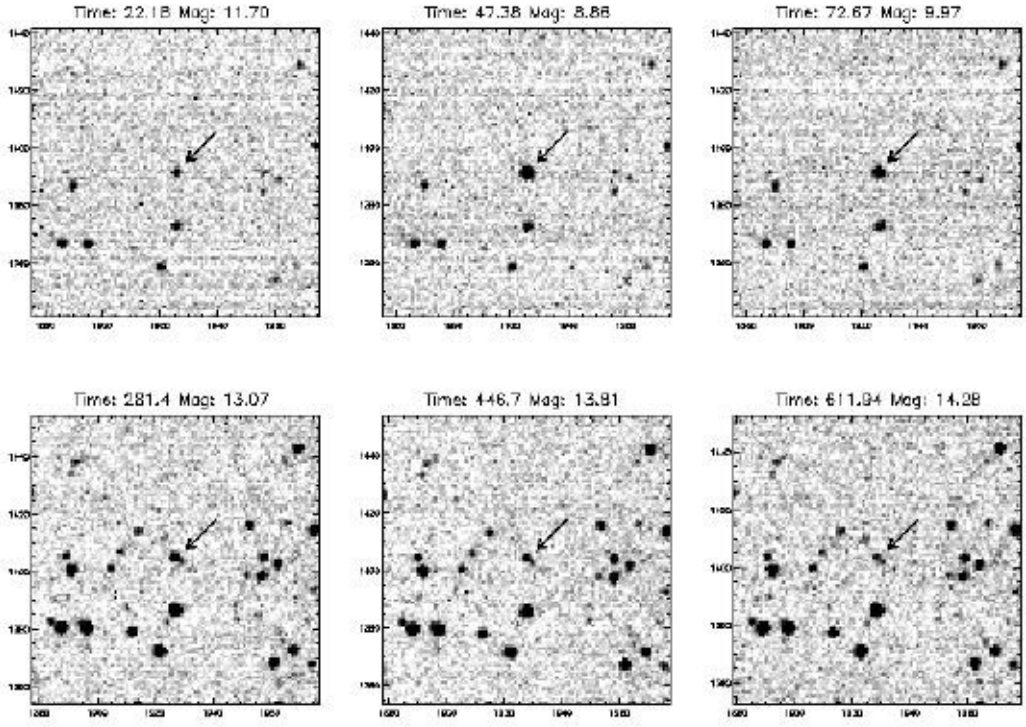

FIGURE 8. 100×100 pixel subimage (24 arcminutes across) surrounding GRB990123 optical counterpart. The top row shows 5 second exposures, while the bottom row shows 75 second exposures.

date	trigger #	loc. source	coverage (%)	dur. (sec.)	rel. fluence (%)
980329a	6665	SAX	100	55	32
980401	6672	IPN	100	37	8
980420	6694	IPN	85 - 100	40	8
980527	6788	BATSE	86	0.1	1
980627	6880	IPN	60	14	1
981121	7219	IPN	68 - 100	60	7
981223	7277	IPN	100	60	13

TABLE 1. Characteristics of seven bursts responded to by ROTSE-I. The second column gives the BATSE trigger number. The third column specificies the origin of the best localization. The fourth column indicates the coverage of the GRB probability in percent. The fifth column indicates the duration in seconds. The last column indicates the fluence of the burst as a percent of GRB990123.

0.1° wide (Hurley et al. (1998)). The intersection of the BATSE position probability distribution with such an 'Interplanetary Network' (IPN) timing annulus produces an IPN arc. The downside to restricting ourselves to using these localizations is that they cannot be obtained for GRBs on the faint end of the BATSE fluence distribution.

We are currently using several analysis strategies to check the consistency of our methods. The simplest is a lightcurve analysis which looks for sources varying by > 2 mag-

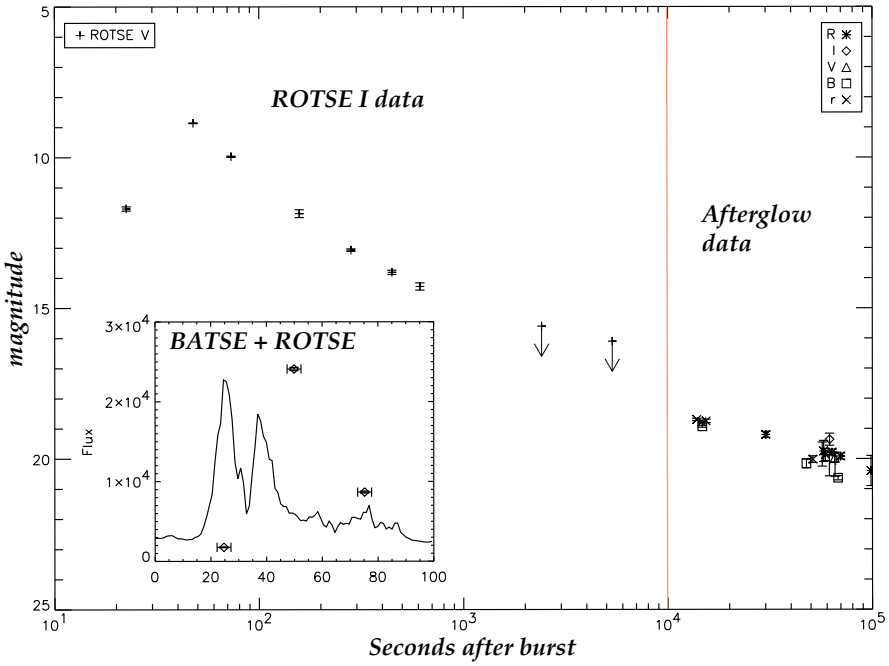

FIGURE 9. Lightcurve from ROTSE-I observations with some early afterglow points. The inset superimposes the first three ROTSE points on the BATSE gamma-ray lightcurve. The vertical line dividing the ROTSE data from the afterglow observations indicates approximately when the earliest arcminute positions can be made available.

nitudes in a trigger response. We also match our object lists to more complete catalogs such as USNO (Monet et al. (1998)) to identify any new objects. The most sensitive method we employ is image differencing. A template for our trigger response images is constructed from precursor sky patrol images and subtracted from the triggered data. If we do not have a very precise localization such as from an X-ray, optical, or radio counterpart, new or varying objects are only considered bona fide optical counterpart candidates if they appear in at least two successive images. This is to remove the background arising from ghosts, cosmic rays, satellite glints, etc. which show up in nearly every image with the field-of-view of ROTSE-I. If we have an IPN arc, we search through the unconstrained IPN annulus in these images for interesting objects. If no source is found, limits are obtained whenever coverage exceeds 50% of the IPN arc. Our results take the form of average magnitudes, $\langle m_V \rangle_x$, during an exposure length, x, vs. the time, t_+, after the start of the burst. Limits refer to the faintest $\langle m_V \rangle_x$ to which we are $> 50\%$ efficient at finding objects after our analysis selection. Unless specifically noted, they do not correspond to long integration times (ie. hundreds of seconds) obtained from co-adding multiple images. The results discussed here are preliminary, and a final, more robust analysis will exploit the full sensitivity of the telescope.

5.2. *GRB980329a*

On March 29, 1998, ROTSE-I successfully responded to its first trigger in automation. The first exposure was begun 11.5 seconds after the gamma-ray rise, and the complete response was finished approximately one hour later. Unfortunately, the sky was fairly

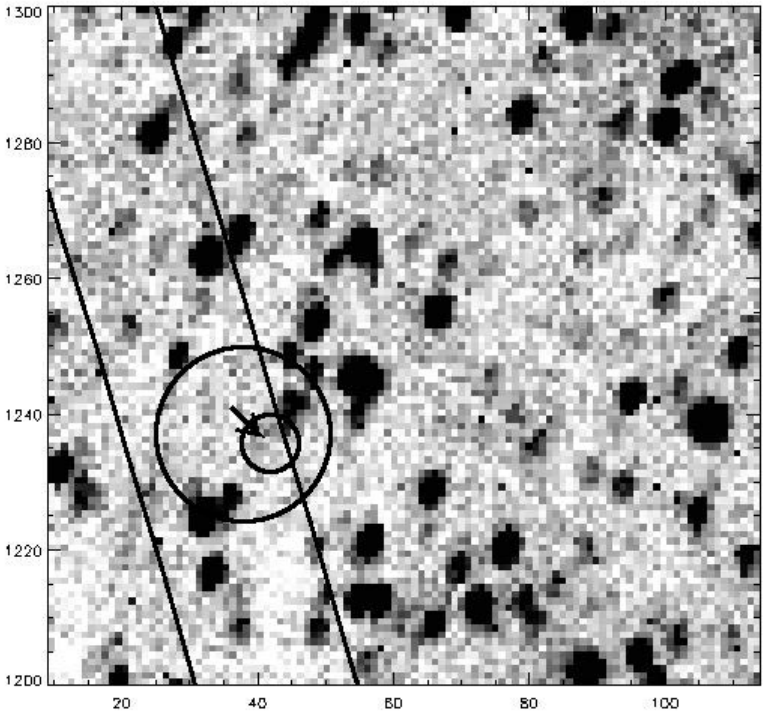

FIGURE 10. Subimage surrounding GRB980329a radio counterpart. Three images were co-added, giving an effective exposure length of 375 seconds. Circles denote the BeppoSAX localizations (Frontera et al. (1998)).

cloudy until the last three frames were taken, and these are somewhat hazy. There were, however, optical (Djorgovski et al. (1998), Palazzi et al. (1998), Pedersen et al. (1998b)), X-ray (Frontera et al. (1998)) and radio (Taylor et al. (1998)) counterparts observed hours later with the result that the burst location is known precisely. Despite the poor quality of the early data, some images are clear enough in the immediate region of the burst to see any 9 - 11 magnitude objects. Since we know exactly where the source is in this case, we use the following reference stars in to estimate the sensitivity of the image in the region: SAO 59687 ($\alpha = 105.297$, $\delta = 39.177$, $m_V = 8.24$), SAO 59692 ($\alpha = 105.308$, $\delta = 38.859$, $m_V = 9.63$), SAO 59708 ($\alpha = 105.585$, $\delta = 39.169$, $m_V = 8.65$) and GSC 958 ($\alpha = 105.583$, $\delta = 38.883$, $m_V = 10.09$). To be conservative, we take the sensitivity to be equal to the magnitude of the dimmest of these objects that can be reliably observed in a given image. The last three images were co-added to produce an image (see Figure 10) sensitive to about 14.8 magnitude as obtained from comparison with the USNO catalog. No object is detected at the known source location in our images. The limits are summarized in Table 2.

5.3. *GRB980401*

Our third trigger, GRB980401, arrived during focusing tests, so a manual response was performed starting 2477 seconds after we received the trigger. This burst has an IPN localization which is completely contained in one camera. The last four 125 second

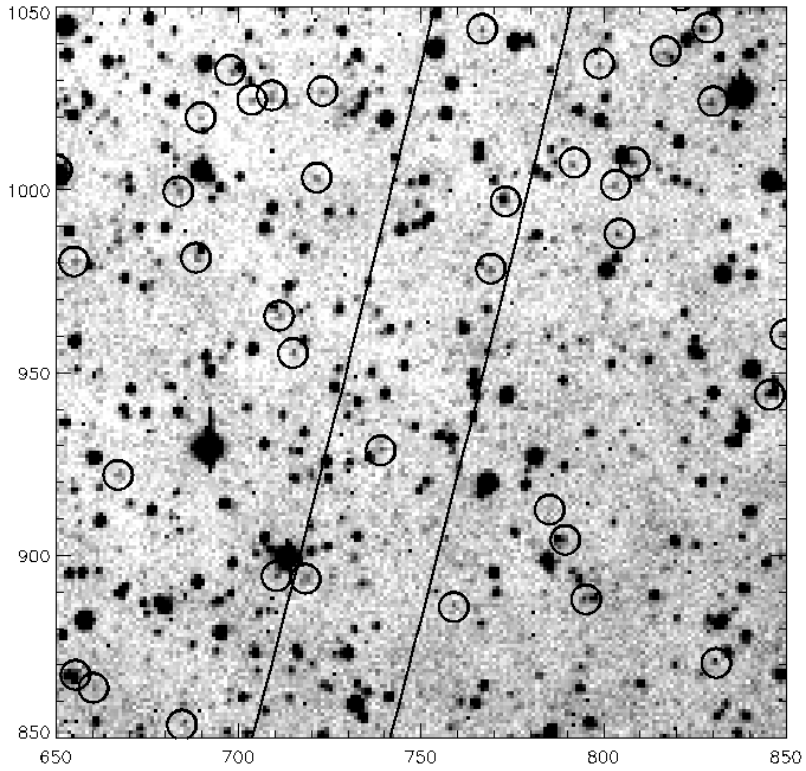

FIGURE 11. Subimage from GRB980401 data with portion of overlapping IPN arc (delineated with solid lines). Circles indicate catalog objects with magnitudes between 16.0 and 16.4.

exposures were co-added into one exposure. While the total exposed time is 500 seconds, the manual nature of the trigger spreads the integration time over about 900 seconds. The resultant image is sensitive to $\langle m_V \rangle_{500} = 16.4$ at $t_+ = 62$ minutes and shows no unkown objects when compared to the USNO catalog (see Figure 11). This is the most stringent optical upper limit on a GRB in the first hour timeframe.

5.4. *GRB980420*

Although conditions for GRB980420 were very good, the camera containing most of the final IPN arc in the initial images was out of focus, thereby greatly reducing the image sensitivity. In tiled and later response images, in-focus cameras overlap the IPN arc resulting in a greater sensitivity. No optical source was observed which varied by more than 2 magnitudes, with an analysis sensitive to 14th magnitude objects in the later images.

5.5. *GRB980527*

While much more difficult, we have begun analyzing bursts for which only BATSE positions are available. Such an analysis requires image differencing to work efficiently. One such burst is GRB980527. The ROTSE-I array covers 100% of the statistical and 86% of the combined statistical and systematic error region, where we have used the systematic error parametrization found in Briggs et al. (1997). The first observation starts at $t_+ =$ 12.6 seconds. Our preliminary analysis is sensitive to $\langle m_V \rangle_5 = 13.0$ and $\langle m_V \rangle_{25} = 14.2$.

date	t_1 (s)	t_{exp1}	$m_V(t_1)$	t_2 (s)	t_{exp2}	$m_V(t_2)$	t_3 (s)	t_{exp3}	$m_V(t_3)$
980329a	51.0	5	9.0	415	25	10.1	2231	375	14.8
980401	-	-	-	-	-	-	3726	500	16.4
980420	31.5	5	9.4	178	5	11.1	2324	125	13.5
980527	14.7	5	13.0	208	25	14.2	-	-	-
980627	-	-	-	180	5	12.2	602	25	12.7
981121	29.7	5	12.8	219	25	13.9	742	125	14.3
981223	24.4	5	12.4	238	25	13.5	-	-	-

TABLE 2. Summary of limits for seven bursts responded to by ROTSE-I. The time an image was taken, the exposure length, and the limiting sensitivity are given. Each time corresponds to the middle of an exposure. Multiple times are listed when the sensitivity significantly improves.

No candidates were found in the early non-tiled images. It should be remembered that this is the only short burst in this sample. The limit of 13.0 at 15 seconds is the best limit obtained by any experiment so soon after a burst.

5.6. *GRB980627*

GRB980627 was fairly dim in gamma-rays and the IPN arc was located very far from the original trigger localization. As a result, a majority of the probability distribution is only covered in our tiled images. No objects were found which varied by more than 2 magnitudes in this data. The images are sensitive to approximately magnitude 12.5, irrespective of exposure length.

5.7. *GRB981121*

We responded to a GRB on November 21, 1998 which was fairly intense in gamma-rays. The data were taken under good conditions, although our shutters were occasionally not opening completely due to very cold weather. Despite this problem, we cover most of the IPN arc for this burst. No unidentified objects were seen with a sensitivity to $\langle m_V \rangle_5 = 12.8$ in early exposures and $\langle m_V \rangle_{25} = 14.3$ in later exposures.

5.8. *GRB981223*

GRB981223 was another burst which was bright in gamma-rays. Our trigger response was prompt and the weather was clear. No unidentified objects were seen with limits in the range 12.4 to 13.5.

6. Results

The preliminary limits placed on the early optical emission for these seven bursts are shown in Figure 12, and a summary of the limit results is given in Table 2. We are able to place a constraint on the overall power-law decline of optical emission from GRB980329a to be shallower than -2.0 with respect to the afterglow points. The best limits are currently $\langle m_V \rangle_5 > 13.0$ at 14.7 seconds for GRB980527, and $\langle m_V \rangle_{500} > 16.4$ at 62 minutes for GRB980401. Given the measurements presented, we can conclude that bright optical counterparts (ie. $m_V \sim 10$) are uncommon.

Now that the optical signature has been seen in one case, the natural question is whether other bursts behave like GRB990123. One way to address this question is to compare optical to gamma-ray levels. To bring all bursts onto some common footing, we

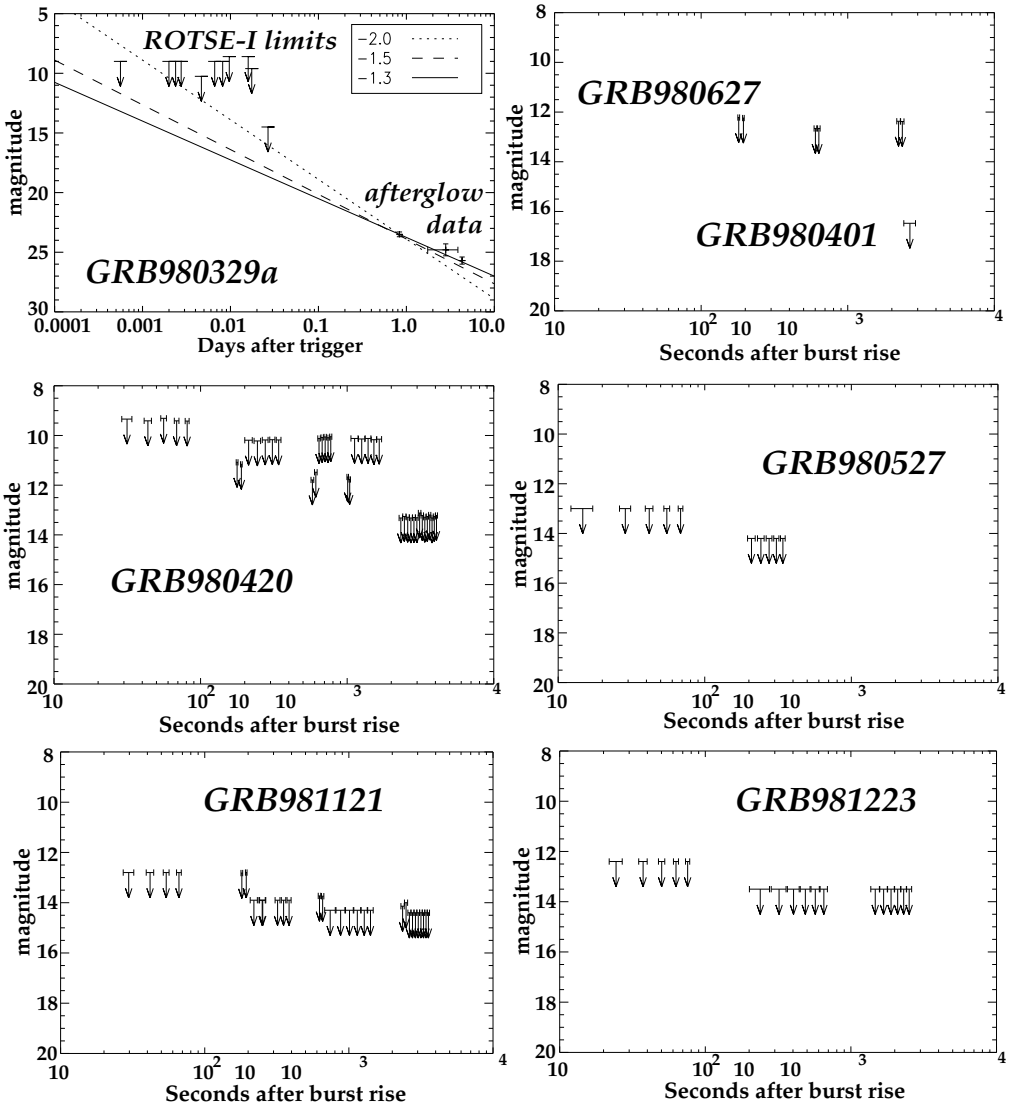

FIGURE 12. Magnitude limits for seven GRB data sets. Each plot shows apparent V band magnitude vs. time after the gamma-ray rise. The time history for GRB980329a has three R-band afterglow observations (Djorgovski et al. (1998), Palazzi et al. (1998), Pedersen et al. (1998b)) superimposed, along with three power law decays passing through the earliest optical detection.

correct for their fluence by defining:

$$\mu \equiv m_V - 2.5 \log(f / f_{GRB990123}), \tag{6.1}$$

where f is the fluence measured in BATSE channels 2 and 3 to avoid systematics due to problems in spectral fitting the other channels (Briggs (1999)).

Several issues of optical extinction arise in our comparison. First, galactic extinction varies significantly over the IPN arcs preventing us from quoting an accurate value in

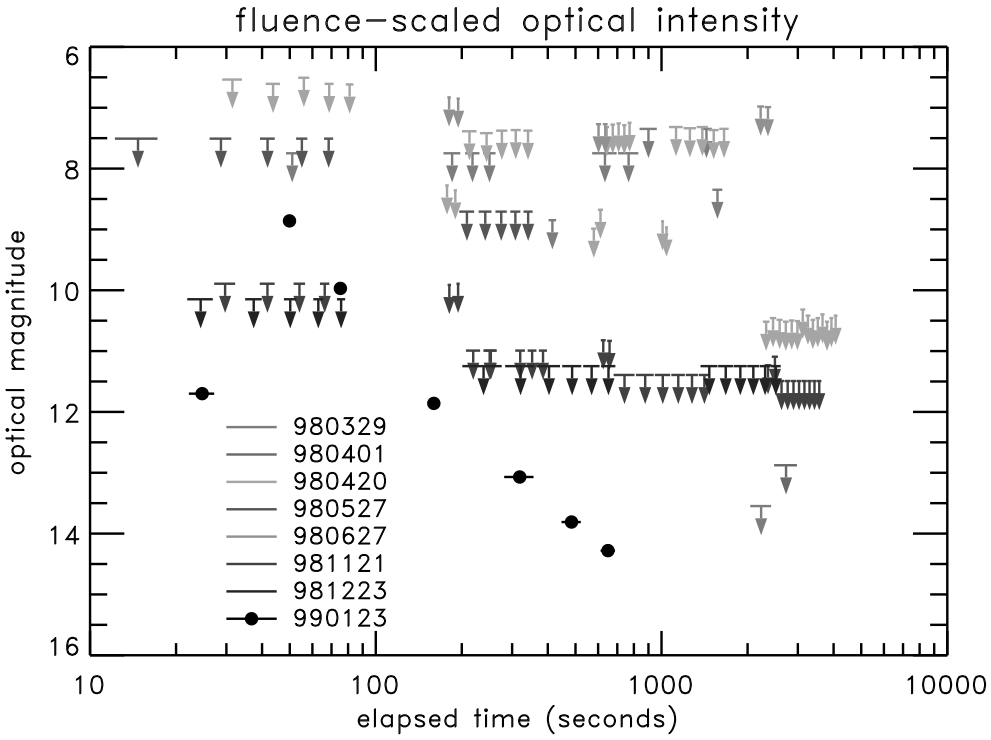

FIGURE 13. Rescaled limits, μ, for seven GRB data sets vs. t_+. Relative to GRB990123, significantly higher optical emission would have been seen during the first few minutes. In two cases, the optical emission is at least one magnitude fainter than GRB990123.

most of the bursts we analyzed. We note, however, that for almost all of these bursts it is much less than 1 magnitude at their most probable location. Since GRB990123 has a similar low value (= 0.04), its effect on our comparison should be minimal. The one exception is GRB980420 which may have over 2 magnitudes of absorption. We ignore the effects of extinction at the source because there is no measure of it in most of these cases, aside from GRB980329a and GRB990123. A statistical argument has been made, however, that most GRBs are not heavily obscured at the source (Frail et al. (1999)).

The limits are replotted as μ vs. t_+ in Figure 13. If the scaled optical emission was much higher than in GRB990123 around $t_+ = 50$ seconds or around $t_+ = 300$ seconds, we would have seen it. In several dimmer bursts, however, we observed no such behavior. While we cannot rule out beaming, there is no evidence for it in this analysis.

More importantly, in two cases, GRB981121 and GRB981223, the optical emission around one minute is at least 1 magnitude fainter than in GRB990123. The main implication of this analysis is that there does not appear to be a strong correlation of optical flux with gamma-ray fluence. The inherent dispersion to any actual correlation must be larger than one magnitude to explain the results from GRB981121 and GRB981223, in particular. A significant correlation, however, is expected in models of reverse-shock development (Sari and Piran (1999)).

There are several caveats and cautions to this analysis. The most important is that

there is a large diversity of GRB behavior. Our results are based on a handful of events, and aside from GRB980527, we are only looking at long bursts. Another limitation arises from the IPN source of final positions, which discriminates against dim bursts. Therefore, our results may not be representative of GRBs in general, and more GRB triggers and further analysis are necessary.

7. Conclusions

We have observed a prompt optical burst during the gamma-ray emission of GRB990123. It is as violent as the burst of gamma-rays, but it displays a different temporal behavior. This difference is consistent with the expected signature of a reverse shock from the explosion.

Preliminary studies of seven other bursts reveal several further points about GRBs. No optical counterparts were identified, and from this we can conclude that bright optical bursts (ie. $m_V \sim 10$) are uncommon. When using fluence as an estimator of total energy output, no bursts with optical flux much greater than GRB990123 have been observed. In two cases, the scaled optical emission around 1 minute is at least 1 magnitude dimmer than for GRB990123. While not conclusive, the non-detection of another optical burst suggests that there is not a strong correlation between gamma-ray and optical emission.

ROTSE is supported by NASA under *SR&T* grant NAG5-5101, the NSF under grants AST-9703282 and AST-9970818, the Research Corporation, the University of Michigan, and the Planetary Society. Work performed at LANL is supported by the DOE under contract W-7405-ENG-36. Work performed at LLNL is supported by the DOE under contract W-7405-ENG-48.

REFERENCES

Akerlof, C. et al. April 1999. Observation of Contemporaneous Optical Radiation from a Gamma-Ray Burst. *Nature.* **398**:400–402.

Barthelmy, S. et al. September 1995. BACODINE, the Real-Time BATSE Gamma-Ray Burst Coordinates Distribution Network. *Astrophysics and Space Science,* **231**:235–238.

Barthelmy, S. et al. 1998. GCN: The GRB Coordinates Network. http://gcn.gsfc.nasa.gov/gcn/.

Bertin, E. and Arnouts, S. 1996. SExtractor: Software for Source Extraction. *Astron. Astrophys. Suppl.,* **117:**393–404.

Briggs, M. et al. 1998. BATSE GRB Location Errors. In C. Meegan, R. Preece, and T. Koshut, ed., *Gamma-Ray Bursts 4th Huntsville Symposium*, 104–108.

Briggs, M. 1999. private communication.

Djorgovski, S. et al. 1998. *GCN Circ.* **41**.

Fenimore, E., Madras, C., and Nayakchin, S. December 1996. *ApJ* **473**:988–1012.

Feroci, M. et al. 1997. In Proc. SPIE Vol. 3114, *EUV, X-ray, and Gamma-Ray Instrumentation for Astronomy VIII*, 186+.

Fishman, G. et al. April 1989. BATSE: The Burst and Transient Source Experiment on the Gamma Ray Observatory. In W. Neil Johnson, ed., *Proc. of the Gamma Ray Observatory Science Workshop*, 2–39.

Frail, D. et al. these proceedings.

Frontera, F. et al. 1998. *IAU Circ.* **6853**.

Fruchter, A. et al. 1998. In C. Meegan, R. Preece, and T. Koshut, ed., *Gamma-Ray Bursts 4th Huntsville Symposium*, 509–515.

Galama, T. et al. 1998. In C. Meegan, R. Preece, and T. Koshut, ed., *Gamma-Ray Bursts 4th Huntsville Symposium*, 478–482.

Hjorth, J. et al. 1999. *GCN Circ.* **219**.

Høg, E. et al. 1998. The Tycho Reference Catalogue. *Astron. Astrophys.* **335**:L65-L68.

Hogg, D. and Fruchter, A. 1999. *ApJ* **520(1)**:54-58.

Hurley, K. et al. July 1984. Astronomical Issues. In E. Liang and V. Petrosian, ed., *Gamma-Ray Bursts*, 3+.

Hurley, K. et al. 1998. GCN/IPN Notices. http://gcn.gsfc.nasa.gov/gcn/ipn.html.

Hurley, K. et al. February 1999. The ULYSSES Supplement to the BATSE 3B Catalog of Cosmic Gamma-Ray Bursts. *ApJ Suppl.* **120**:399–408.

Jager, R. et al. 1997. *Astron. Astrophys. Suppl.* **125**:557–572.

Janka, H. and Ruffert, M. 1996. *Astron. Astrophys.* **307**:L33–L36.

Kelson, D. et al. 1999. *IAU Circ.* **7096**.

Klebesadel, R., Strong, I. and Olson, R.. June 1973. Observations of Gamma-Ray Bursts of Cosmic Origin. *ApJ* **182(2)**:L85–L88.

Kouveliotou, C. et al. August 1993. Identification of Two Classes of Gamma-Ray Bursts. *ApJ* **413**:L101–L104.

Kouveliotou, C. et al. 1996. Correlations between Duration, Hardness, and Intensity in GRBs. In C. Kouveliotou, M. Briggs, and G. Fishman, ed., *Gamma-Ray Bursts 3rd Huntsville Symposium*, 42–46.

Kulkarni, S. et al. 1998. *Nature*, **393**:35–39.

Kulkarni, S. et al. April 1999. The Afterglow, Redshift and Extreme Energetics of the γ-Ray Burst of 23 January 1999. *Nature.* **398**:389–394.

Meegan, C. et al. 1998. The 4B BATSE Gamma-Ray Burst Catalog. In C. Meegan, R. Preece, and T. Koshut, ed., *Gamma-Ray Bursts 4th Huntsville Symposium*, 3–9.

Meszaros, P. and Rees, M. 1993. *ApJ* **405**:278+.

Meszaros, P. and Rees, M. 1997. *ApJ* **482**:L29+.

Metzger et al. 1997. *IAU Circ.* **6676**.

Monet, D. et al. 1998. A Catalog of Astrometric Standards. US Naval Observatory, Washington DC.

Odewahn, S., Bloom, J., and Kulkarni, S. 1999. *GCN Circ.* **201**.

Palazzi, E. et al. 1998. *GCN Circ.* **48**.

Paczynski, B. and Xu, G. June 1994. *ApJ* **427**:708-713.

Pedersen, H. et al. 1998. In C. Meegan, R. Preece, and T. Koshut, ed., *Gamma-Ray Bursts 4th Huntsville Symposium*, 530–534.

Pedersen, H. et al. 1998. *GCN Circ.* **52**.

Piro, L. et al. 1999. *GCN Circ.* **199**.

Rees, M. and Meszaros, P. July 1992. *Mon. Not. R. Astro. Soc.* **258**:41–43.

Rees, M. and Meszaros, P. August 1994. *ApJ* **430(2)**:L93–L96.

Rhoads, J. 1999. *astro-ph* **9903399**.

Ricker et al. July 1990. In C. Ho, R. Epstein, and E. Fenimore, ed., *Gamma-Ray Bursts Observations, Analyses and Theories.*

Ruffert, M. et al. 1997. *Astron. Astrophys.* **319**:122–153.

Sari, R. and Piran, T. 1999. *ApJ.* **517(2)**:L109–L112.

Taylor, G. et al. 1998. *GCN Circ.* **40**.